C–H Bond Activation

DOI: 10.1002/ange.201200045

Synergistic Effect on the Photoactivation of the Methane C–H Bond over Ga^{3+}-Modified ETS-10**

*Lu Li, Yi-Yu Cai, Guo-Dong Li, Xiao-Yue Mu, Kai-Xue Wang, and Jie-Sheng Chen**

During the past decades, many efforts have been devoted to activation of the strong C–H bond in methane under mild conditions[1–4] because through suitable conversion methane may be used to substitute for the dwindling petroleum resources as a chemical feedstock. Among the various strategies is a compelling approach that uses photoenergy to drive the conversion of methane to more valuable molecules through dehydrogenation at room temperature. Yoshida et al. developed several effective photocatalysts, such as the ternary oxide SiO_2–Al_2O_3–TiO_2,[5] for methane conversion. Recently, we used zinc to modify the medium-pore ZSM-5 zeolite and found that the resulting material exhibits substantial photocatalytic activity for the selective conversion of methane to ethane and hydrogen under ultraviolet (UV) irradiation.[6] However, there are still huge challenges in finding more powerful systems to achieve a practical product yield and to exploit solar energy more effectively for the photodriven conversion of methane. It is now a consensus that the H_3C–H bond cleavage process is a key step in the dehydrogenation and dimerization of methane.[7,8] Investigations into this process provide insights into the essence of methane conversion at a molecular level, and thus enable us to design better performing systems. Nevertheless, only limited information about the mechanism for the photoinduced cleavage of the H_3C–H bond occurring on substrate surfaces has been revealed so far,[9] and the nature of the photoactive species responsible for the methane C–H activation has yet to be elucidated in more detail. Previously, two models for the photoactivation of the methane C–H bond were proposed. One considers that the presence of oxygen-centered radicals brings about homolytic C–H bond cleavage,[10] whereas in the other highly dispersed metal species are believed to be the active sites of methane dehydrogenation.[6,11]

Herein, we describe a Ga^{3+}-modified ETS-10 zeolite material (ETS-10 = titanosilicate) in which the photogenerated hydroxyl radical and the extraframework metal ion interact with the methane molecule to split the H_3C–H bond in a synergistic way under UV irradiation ($\lambda < 350$ nm). It is demonstrated that the combination of both oxygen-centered and metal-centered active sites in the material significantly enhances its photoactivity for methane C–H bond activation, leading to efficient non-oxidative coupling of methane at room temperature. An average methane conversion rate of around 29.8 $\mu mol\,h^{-1}\,g^{-1}$ was achieved after UV irradiation for 5 h, which is 3 and 20 times faster than those of Zn^+-modified ZSM-5 zeolite and SiO_2-Al_2O_3-TiO_2 material (the two best photocatalysts for methane conversion developed so far), respectively.

ETS-10 is a microporous titanosilicate with a framework containing one-dimensional O-Ti-O-Ti-O semiconducting nanowires (diameter of 0.67 nm) insulated from one another by the surrounding SiO_2 matrix (Figure 1).[12] The combination of quantum-confined titanate wires, uniform pore structure, and the presence of nonframework cations renders

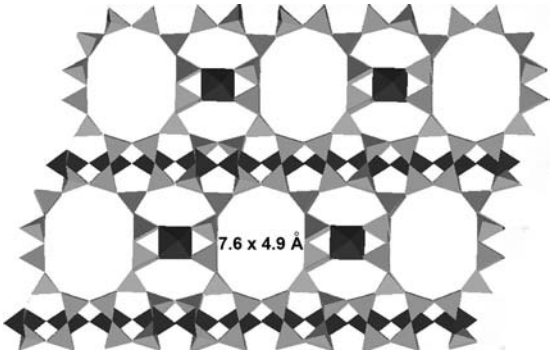

Figure 1. Framework structure of ETS-10. The TiO_3^{2-} quantum wires are shown in black and the SiO_4 tetrahedra in gray. The extraframework cations (Na^+ and K^+) are not indicated for clarity.

ETS-10 attractive for photoactivation applications.[13] The incorporation of extra metal ions into ETS-10 either through ion exchange[14] or through isomorphous substitution[15] enhances its photoactivity. The unusual attributes of ETS-10 prompted us to explore its potential to photoactivate the C–H bond in methane.

Ion exchange of zeolites with metal-salt solutions is a simple and effective route for the preparation of zeolites containing extraframework metal cations. Through ion exchange, we have prepared a series of M-ETS-10 (M = extraframework Ga^{3+}, Al^{3+}, Zn^{2+}, Fe^{3+}, and Cu^{2+} cations) samples with various metal contents. The ETS-10 precursor ((Na,K)-ETS-10) has a composition of $(Na_{0.78},K_{0.22})_2TiSi_5O_{13}$ and a Brunauer–Emmett–Teller (BET) surface area of 331 $m^2\,g^{-1}$. For clarity, the corresponding metal-exchanged

[*] L. Li, Y. Y. Cai, Prof. K. X. Wang, Prof. J.-S. Chen
School of Chemistry and Chemical Engineering
Shanghai Jiao Tong University
Shanghai 200240 (P.R. China)
E-mail: chemcj@sjtu.edu.cn
L. Li, Prof. G. D. Li, X. Y. Mu
State Key Laboratory of Inorganic Synthesis and Preparative Chemistry, College of Chemistry
Jilin University, Changchun 130012 (P.R. China)

[**] This work was financially supported by the NSFC and the National Basic Research Program of China (2011CB808703).

Supporting information for this article is available on the WWW under http://dx.doi.org/10.1002/anie.201200045.

ETS-10 products are designated M-ETS-10-X with M and X standing for the particular exchanged metal and the concentration of the metal solution used for the ion exchange, respectively. As shown in Figure 2a, none of the corresponding aggregates of metal oxide or metal salt impurities was

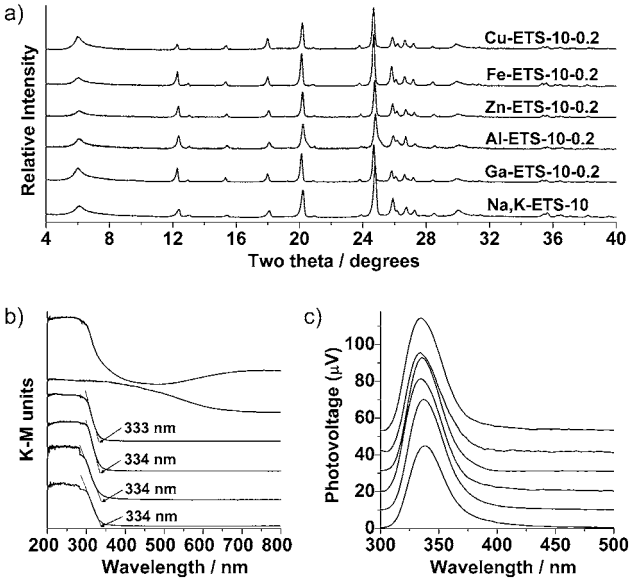

Figure 2. a) Powder X-ray diffraction patterns of various metal-exchanged ETS-10 samples and their corresponding b) UV/Vis diffuse reflectance spectra (K-M units = Kubelka–Munk units) and c) surface photovoltage spectra under zero external bias. From bottom to top: pristine (Na,K)-ETS-10, Ga-ETS-10-0.2, Al-ETS-10-0.2, Zn-ETS-10-0.2, Fe-ETS-10-0.2, and Cu-ETS-10-0.2.

detected in the X-ray powder diffraction patterns of these metal-exchanged ETS-10 samples. According to inductively coupled plasma (ICP) elemental analysis and he powder X-ray fluorescence (XRF) spectroscopy, the composition of Ga-ETS-10-0.2 is $(Na,K)_{0.29}Ga_{0.57}TiSi_5O_{13}$. The compositions of other metal-exchanged ETS-10 materials are presented in the Supporting Information (Table S1). Furthermore, all the gallium ions in Ga-ETS-10-0.2 were found to be trivalent by using the X-ray photoelectron spectroscopy (XPS) technique (Figure S1).[16]

The optical properties of the as-prepared metal-exchanged samples were probed by UV/Vis diffuse reflectance and surface photovoltage (SPV) spectroscopy. As shown in the UV/Vis spectra (Figure 2b), the pristine ETS-10 and Ga^{3+}-, Al^{3+}-, and Zn^{2+}-exchanged ETS-10 samples exhibit absorption bands only in the UV range with a threshold at 334 nm, which is attributed to the O(2p) to Ti(3d) charge-transfer (CT) transitions;[17] whereas the Fe^{3+}- and Cu^{2+}-ETS-10 materials have significant absorption bands in the visible region other than that in the UV region. These visible absorption bands correspond to the d–d transitions in Fe^{3+} and Cu^{2+} cations, respectively. In contrast, the SPV spectra are associated with separation of photogenerated charges (electrons and holes) and d–d transitions in transition-metal ions do not contribute to the SPV signals. All the ETS-10 based materials before and after ion exchange gave similar SPV responses ranging from 300 to 380 nm with peak maxima at around 334 nm (Figure 2c). These observations demonstrate that the incorporation of the extraframework metal cations into ETS-10 through ion exchange has little effect on the bandgap of the ETS-10 host. In contrast, isomorphous substitution of framework Si or Ti atoms by other metal is capable of shifting the band gap of ETS-10.[15]

The performances of the metal-exchanged ETS-10 materials for the photodriven methane activation reaction were tested at room temperature with UV irradiation from a 150-W high-pressure Hg lamp (Table S1 and Figure S2). A freshly-prepared sample (0.2 g) was spread evenly on the wall of an air-tight quartz reactor in vacuum (see Figure S3 in the Supporting Information), followed by introduction of pure methane (200 μmol; > 99.995% purity). To avoid the influence of ion exchange on the nature of the ETS-10 host, the pristine ETS-10 before the test was also subjected to ion-exchange treatment with 0.2 M sodium nitrate solution (15 mL), and the resulting material is designated Na,K-ETS-10-0.2. Figure 3 and Table S1 present the results of methane conversion over various substrates after ion

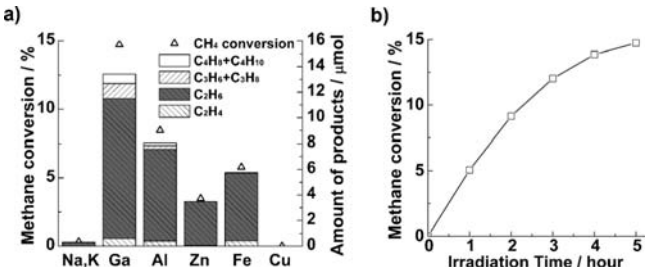

Figure 3. a) Methane conversion and product distribution obtained in the photodriven methane activation reaction over various substrates under direct irradiation from a high-pressure Hg lamp over 5 h. From left to right: Na,K-ETS-10-0.2, Ga-ETS-10-0.2, Al-ETS-10-0.2, Zn-ETS-10-0.2, Fe-ETS-10-0.2, and Cu-ETS-10-0.2; b) methane conversion as a function of time over Ga-ETS-10-0.2 under direct irradiation from high-pressure Hg lamp. Modified zeolite material (0.2 g) and methane (200 μmol) were used in all cases.

exchange. Ga-ETS-10-0.2 is the best material for methane conversion among all the samples tested. Several hydrocarbon products (C_2 to C_4) with a selectivity larger than 70% for ethane were obtained from the reaction systems. Carbon mass balances during the reaction are close to 100%, and no carbon oxides were detected by gas chromatography. In addition, the reaction does not proceed at all in the dark at room temperature, indicating that the non-oxidative methane conversion reaction over the ETS-10 based solids is light-driven.

After UV irradiation for 5 h, 14.9% of methane was consumed by Ga-ETS-10-0.2 (Table S1, entry 1), corresponding to a methane conversion rate of 29.8 $\mu mol\,h^{-1}\,g^{-1}$. For comparison, under similar conditions, the methane conversion rates for the Zn^{+}-modified ZSM-5 zeolite and SiO_2-Al_2O_3-TiO_2 were reported previously to be 9.8 and 1.33 $\mu mol\,h^{-1}\,g^{-1}$, respectively. With increasing reaction time, the produced ethane can react further with Ga-ETS-10-0.2 to

form other hydrocarbons so that the content of ethane in the product decreases whereas those of higher hydrocarbons increase. To confirm this observation, pure ethane instead of methane was used as the reactant. Using 0.2 g of Ga-ETS-10-0.2 and 200 μmol of ethane, a conversion of 11.0% and a butane selectivity of 57% were achieved after UV irradiation for 5 h (Table S1, entry 2). This result demonstrates that the Ga^{3+}-exchanged ETS-10 material can also activate the C–H bond in ethane under UV irradiation. Furthermore, no hydrocarbons larger than butane ($>C_4$) were observed in the reaction product in this case because of the restriction of the pore size of the ETS-10 host.

Using a series of UV-cut-out filters, we determined that the minimum light energy required to drive the methane-activation reaction over Ga-ETS-10-0.2 corresponds to a wavelength of about 350 nm. To evaluate quantitatively the performance of Ga-ETS-10-0.2 upon UV irradiation within the wavelength range 300–400 nm, a UV-D35 filter (Figure S4) was carefully mounted in the system to block completely wavelengths shorter than 300 nm and longer than 400 nm from the high-pressure Hg lamp. Using 0.2 g of Ga-ETS-10-0.2 and 200 μmol of methane gave a conversion of 12.8% after irradiation for 24 h (Table S1, entry 3).

Besides Ga^{3+}-modified ETS-10, Al^{3+}-, Zn^{2+}-, and Fe^{3+}-modified ETS-10 were also effective in promoting the methane activation reaction (Figure 3a and Table S1, entries 4–6). In contrast, the activities of (Na^+,K^+)- and Cu^{2+}-modified ETS-10 were distinctly low (Table S1, entries 7 and 8). In the case of Ga^{3+}-modified ETS-10, the higher the content of Ga^{3+} cations, the higher the conversion of methane (Table S1, entries 9–11). These observations demonstrate that the modification metal ions play an important role in the photodriven methane-activation reaction.

The dependence of the methane consumption upon the initial irradiation time (0–60 s) is presented in Figure S5. The result demonstrates that the Ga-ETS-10 material shows activity for methane conversion immediately upon exposure to the UV irradiation, and the rate of methane consumption remains constant. No induction period was observed. However, the oxidation state of the trivalent gallium center in the Ga-ETS-10 material remains unchanged during the methane photoactivation process, as shown by X-ray photoelectron spectroscopy. After UV irradiation for 5 h in the presence of methane, the XPS spectrum for the Ga-ETS-10 material was essentially the same as that for the parent Ga-ETS-10; neither of the binding energy peaks with maxima at 19.1 (typical for Ga^+) and 17.7 eV (typical for Ga^0)[16] was detected, and the only gallium signal (21.2 eV) in the XPS spectrum (see Figure S1) corresponds to Ga^{3+} species. These results indicate that the Ga^{3+} cations in Ga-ETS-10 are not reduced to become additional active centers during the photodriven methane activation reaction at room temperature.

To evaluate the effect of the zeolite host on the photoactivation of the methane C–H bond, two aluminosilicate zeolites ZSM-5[6] and Y[18] were used as host materials in place of ETS-10 for the preparation of Ga^{3+}-containing samples by ion exchange (Figure S6). The photoactivities of Ga^{3+}-exchanged ZSM-5 and Y samples were very poor for methane conversion (Table S1, entries 12 and 13), although the content of Ga^{3+} ions in Ga-Y-0.2 is comparable with that in Ga-ETS-10-0.2. Evidently, the presence of photoactive TiO_2 units in the host framework is crucial for the photodriven methane conversion reaction, and the possibility that the excellent activity of Ga-ETS-10-0.2 for photodriven methane conversion arises from one single factor (the semiconducting titanate wires or the extraframework Ga^{3+} cations) can be ruled out. Presumably, the combination of the two factors in the photodriven reaction results in the efficient methane C–H bond activation.

In the ideal structure of ETS-10, the titanate wires are surrounded by SiO_4 tetrahedra, and in principle they are not accessible to extraframework species. Nevertheless, there exist structural defects in ETS-10 where titanium sites are exposed, and guest species may get access to these sites. Raman spectroscopy is very sensitive to the state of the titanate wires in ETS-10 (Figure S7); the pristine ETS-10 material without ion-exchange treatment gives an intense Raman band at 727 cm^{-1}, corresponding to the stretching vibrations of the titanate wires.[19] However, after ion exchange, this band decreases in intensity and its maximum shifts toward higher frequency, suggesting that the length and the coordination of the titanate wires varied significantly.[20] The ion-exchange treatment brings structural defects along the titanate wires, resulting in much more accessible Ti ions, which are coordination-saturated by hydroxy groups (Ti–OH).[13,14] As shown in the infrared (IR) spectra (Figure S8), the pristine ETS-10 without ion exchange has only one absorption band at 3734 cm^{-1} between 4000 and 3000 cm^{-1}, corresponding to the stretching vibration of surface Si–OH, whereas the metal-exchanged ETS-10 samples have additional absorptions that are attributed to the stretching vibration of Ti–OH groups.[20]

The as-prepared Ga-ETS-10-0.2 sample shows no electron paramagnetic resonance (EPR) signals either before or after UV irradiation, indicating that no unpaired electrons are present. However, upon UV irradiation in the presence of methane, the initially EPR-silent sample exhibits a distinct EPR signal that is characteristic of Ti^{3+} cation with an axial g tensor ($g_\perp = 1.962$, $g_\parallel = 1.937$),[21] and this signal increases in intensity with irradiation time (Figure 4a). Presumably, when Ga-ETS-10-0.2 is exposed to UV irradiation in the presence of methane, the photogenerated charge carriers (electrons and holes) from the semiconducting titanate wires migrate rapidly to the surface (either internal or external) of the zeolite material and are trapped by the Ti–OH moieties.[13] The holes are captured by the OH groups, producing hydroxyl radicals (·OH), whereas the photogenerated electrons are trapped at the Ti^{4+} sites to form Ti^{3+} ions. The ·OH radical abstracts a hydrogen atom from methane to form water,[10] leaving $·CH_3$ radicals, which then combine to release as ethane. The disappearance of Ti–OH groups and the formation of water during the methane activation reaction were shown by in situ IR spectroscopy (Figure S8).

However, as mentioned earlier, only in the presence of some particular extraframework metal ions (Ga^{3+}, Al^{3+}, Zn^{2+}, and Fe^{3+}) is the photoactivity of the ETS-10 host for the methane conversion reaction significantly enhanced, whereas the Na^+, K^+, and Cu^{2+} cations are not able to promote the

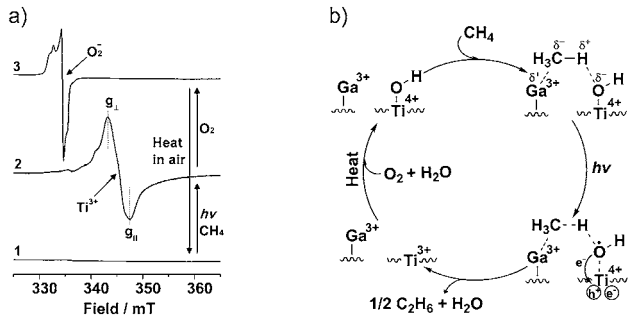

Figure 4. a) Room-temperature X-band EPR spectra of Ga-ETS-10-0.2 in vacuum (curve 1), under UV irradiation in the presence of methane (curve 2), and followed by exposure to oxygen (curve 3); b) reaction mechanism involved in the photodriven methane activation reaction.

photodriven reaction. Previously, Ga^{3+}, Al^{3+}, Zn^{2+}, and Fe^{3+} have been proved to be capable of adsorbing methane dissociatively and forming metal–methyl intermediates at elevated temperatures,[8] and Na^+, K^+, and Cu^{2+} ions do not have this function.[22] Even at room temperature, the polarization of alkane C–H bonds by Ga^{3+} cations is very strong. This is evidenced by the observation that the C–H symmetric stretching mode of saturated alkane (IR symmetry forbidden for the free molecule) becomes IR active and shifts much toward lower frequencies ($>100\ cm^{-1}$) upon interaction with cations such as Ga^{3+}.[23,24] As the adsorbed methane is polarized by the interaction between the individual metal ion (Ga^{3+}, Al^{3+}, Zn^{2+}, and Fe^{3+} in our case) and the methyl group ($\cdot M^{n+}\cdots C^{\delta-}-H^{\delta+}$),[25] the C–H bond is significantly weakened, promoting the hydrogen abstraction from methane by the ·OH radicals in the vicinity. Thus, the photodriven cleavage of the H_3C-H bond is in fact a synergistic process of photogenerated ·OH radicals and extraframework metal cations (Figure 4b).

Thermal treatment of the Ti^{3+}-containing Ga-ETS-10-0.2 sample in the presence of oxygen and water at about 250 °C for 2 h leads to recovery of the Ti–OH groups in the material (Figure 4a and Figure S8), and, as a result, the photoactivity of the sample is regained. During the treatment, the photogenerated Ti^{3+} ion transfers its electron to oxygen to form superoxide O_2^- (Figure 4a), which further interacts with water to produce hydroxyl radicals[13,26] at an elevated temperature (250 °C in our case). The performance of Ga-ETS-10-0.2 for the photodriven conversion of methane was tested for five cycles (Figure S9), and the results indicate that the material may be used repeatedly without noticeable deactivation after the simple thermal treatment in moist air. After the repeated tests, the crystal structure of the sample remained intact, as judged by powder X-ray diffraction (Figure S10).

The key to the excellent performance of Ga-ETS-10-0.2 for the photodriven methane activation reaction is the presence of binary active species, that is, the extraframework metal cations and the Ti–OH groups on titanate wires, which interact with methane in a synergistic manner under UV irradiation, leading to easy cleavage of the methane C–H bond. In comparison with the materials bearing only one active species (Na^+, K^+, and Cu^{2+} modified ETS-10 or Ga^{3+}-modified Y and ZSM-5), the photoactivity of Ga-ETS-10-0.2 for methane conversion is enhanced by at least a factor of 27 under identical reaction conditions.

Experimental Section

Preparation of (Na^+,K^+)-, Ga^{3+}-, Al^{3+}-, Zn^{2+}-, Fe^{3+}-, and Cu^{2+}-modified ETS-10 samples: The details for the preparation of the metal-exchanged ETS-10 materials are described in the Supporting Information.

Photodriven methane activation reaction: All tests were performed under a dry Ar atmosphere or in a vacuum using Schlenk glassware, glove-box, or vacuum-line techniques. All the reactants were dried by passing the corresponding gases through a column of $MgSO_4$ and $CuSO_4$ prior to catalytic testing. The activity for the photodriven methane activation reaction was evaluated in an airtight quartz reactor (20 cm^3) at room temperature. Solid material (0.2 g) was spread evenly on the wall of a closed quartz reactor, which was then evacuated at 250 °C for 2 h to remove water and other molecules adsorbed in the zeolitic material. Afterwards, the reactor was cooled slowly to room temperature under vacuum ($P < 0.01$ Pa), followed by reaction with pure methane (200 μmol) under UV irradiation from a 150 W high-pressure Hg lamp for 5 h. The light intensity of the high-pressure Hg lamp was measured to be approximately 100 mW cm^{-2}. If a UV-D35 filter ($300\ nm < \lambda_{transmittance} < 400\ nm$) was used, the light intensity measured at wavelengths between 300 and 400 nm was around 2.5 mW cm^{-2}. The hydrocarbon products were thermally desorbed by heating the reactor gradually up to 250 °C and continuing heating for 60 min under evacuation, collected with a liquid-N_2 trap, and analyzed by gas chromatography (GC) with a flame-ionization detector (FID). The amounts of carbon oxides or hydrogen (if any) were measured directly by GC with a thermal conductivity detector (TCD).

General characterization: Powder X-ray diffraction (XRD) patterns were recorded on a Rigaku D/Max 2550 X-ray diffractometer with $Cu_{K\alpha}$ radiation ($\lambda = 1.5418$ Å). EPR spectra were obtained on a JES-FA 200 EPR spectrometer; scanning frequency: 9.45 GHz; central field: 340 mT; scanning width: 500 mT; scanning power: 0.998 mW; scanning temperature: 25 °C. The stable radical 2,2-diphenyl-1-picrylhydrazyl (DPPH) was used as a standard for the calculation of g values. X-ray photoelectron spectroscopy (XPS) was performed on an ESCALAB 250 X-ray photoelectron spectrometer with a monochromated X-ray source ($Al_{K\alpha}$ $h\nu = 1486.6$ eV). The energy scale of the spectrometer was calibrated using $Au4f_{7/2}$, $Cu2p_{3/2}$, and $Ag3d_{5/2}$ peak positions. The standard deviation for the binding energy (BE) values was 0.1 eV. For in situ infrared spectral measurements, a thin self-supporting wafer (10–15 mg cm^{-2}) of the sample was evacuated in the preheating zone of a home-made IR cell by heating the sample to 250 °C for 2 h. Upon cooling to room temperature, the sample was lowered from the preheating zone into the sample compartment for the IR measurement. The sample in the IR cell was then exposed to methane under UV irradiation, and the IR spectrum was recorded again for comparison after reaction. All the FTIR spectra were recorded on a Bruker IFS 66v/S FTIR spectrometer equipped with a deuterated triglycine sulfate (DTGS) detector. UV/Vis diffuse reflectance spectra were recorded on a Perkin–Elmer Lambda 20 UV/Vis spectrometer, whereas the UV/Vis absorption spectrum of the filter was measured with a Shimadzu UV-2450 spectrophotometer. The absorbance spectra were obtained from the reflectance ones through Kubelka–Munk transformation. The surface photovoltage spectroscopy (SPS) measurement system consisted of a source of monochromatic light, a lock-in amplifier (SR830-DSP) with a light chopper (SR540), a photovoltaic cell, and a computer. A 500-W xenon lamp and a grating monochromator (Omni-λ 500) were combined to provide the monochromatic light. A low chopping frequency of 23 Hz was used to obtain stable and intensive signals.

The photovoltaic cell was a sandwich-like structure consisting of ITO–sample–ITO (ITO = indium tin oxide). Raman spectra were obtained with a Renishaw inVia confocal Raman spectrometer, and 532 nm radiation from a solid-state laser was used as the exciting source (350 mW). ICP elemental analyses were performed on a Perkin–Elmer Optima 3300DV ICP spectrometer, and X-ray fluorescence spectra were collected on a Panalytical Axios spectrophotometer equipped with a rhodium tube as the source of radiation. The Brunauer–Emmett–Teller (BET) surface areas of the samples were measured from the adsorption of N_2 at 77 K by using a Micromeritics ASAP 2020M system.

Received: January 3, 2012

Keywords: C–H activation · gallium · ion exchange · photochemistry · silicates

[1] J. H. Lunsford, *Catal. Today* **2000**, *63*, 165 – 174.
[2] R. A. Periana, O. Mironov, D. Taube, G. Bhalla, C. J. Jones, *Science* **2003**, *301*, 814 – 818.
[3] A. Holmen, *Catal. Today* **2009**, *142*, 2 – 8.
[4] R. Balasubramanian, S. M. Smith, S. Rawat, L. A. Yatsunyk, T. L. Stemmler, A. C. Rosenzweig, *Nature* **2010**, *465*, 115 – 119.
[5] H. Yoshida, N. Matsushita, Y. Kato, T. Hattori, *J. Phys. Chem. B* **2003**, *107*, 8355 – 8362.
[6] L. Li, G. D. Li, C. Yan, X. Y. Mu, X. L. Pan, X. X. Zou, K. X. Wang, J. S. Chen, *Angew. Chem.* **2011**, *123*, 8449 – 8453; *Angew. Chem. Int. Ed.* **2011**, *50*, 8299 – 8303.
[7] N. Dietl, M. Engeser, H. Schwarz, *Angew. Chem.* **2009**, *121*, 4955 – 4957; *Angew. Chem. Int. Ed.* **2009**, *48*, 4861 – 4863.
[8] C. Copéret, *Chem. Rev.* **2010**, *110*, 656 – 680.
[9] L. Yuliati, H. Yoshida, *Chem. Soc. Rev.* **2008**, *37*, 1592 – 1602.
[10] C. E. Taylor, *Catal. Today* **2003**, *84*, 9 – 15.
[11] L. Yuliati, T. Hamajima, T. Hattori, H. Yoshida, *J. Phys. Chem. C* **2008**, *112*, 7223 – 7232.
[12] M. W. Anderson, O. Terasaki, T. Ohsuna, A. Philippou, S. P. Mackay, A. Ferreira, J. Rocha, S. Lidin, *Nature* **1994**, *367*, 347 – 351.
[13] F. X. Llabrés i Xamena, P. Calza, C. Lamberti, C. Prestipino, A. Damin, S. Bordiga, E. Pelizzetti, A. Zecchina, *J. Am. Chem. Soc.* **2003**, *125*, 2264 – 2271.
[14] P. K. Surolia, R. J. Tayade, R. V. Jasra, *Ind. Eng. Chem. Res.* **2010**, *49*, 3961 – 3966.
[15] A. M. Shough, D. J. Doren, *Chem. Mater.* **2009**, *21*, 1232 – 1241.
[16] A. I. Serykh, M. D. Amiridis, *Surf. Sci.* **2009**, *603*, 2037 – 2041.
[17] A. M. Shough, R. F. Lobob, D. J. Doren, *Phys. Chem. Chem. Phys.* **2007**, *9*, 5096 – 5104.
[18] L. Li, X. S. Zhou, G. D. Li, X. L. Pan, J. S. Chen, *Angew. Chem.* **2009**, *121*, 6806 – 6810; *Angew. Chem. Int. Ed.* **2009**, *48*, 6678 – 6682.
[19] N. C. Jeong, H. Lim, H. Cheong, K. B. Yoon, *Angew. Chem.* **2011**, *123*, 8856 – 8860; *Angew. Chem. Int. Ed.* **2011**, *50*, 8697 – 8701.
[20] M. J. Nash, R. F. Lobo, D. J. Doren, *Appl. Catal. B* **2009**, *88*, 232 – 239.
[21] Y. K. Krisnandi, R. F. Howe, *Appl. Catal. A* **2006**, *307*, 62 – 69.
[22] T. Tabata, M. Kokitsu, O. Okada, *Catal. Lett.* **1994**, *25*, 393 – 400.
[23] A. M. Ferrari, S. Huber, H. Knözinger, K. M. Neyman, N. Rösch, *J. Phys. Chem. B* **1998**, *102*, 4548 – 4555.
[24] V. B. Kazansky, I. R. Subbotina, A. A. Pronin, R. Schlögl, F. C. Jentoft, *J. Phys. Chem. B* **2006**, *110*, 7975 – 7978.
[25] M. V. Luzgin, A. A. Gabrienko, V. A. Rogov, A. V. Toktarev, V. N. Parmon, A. G. Stepanov, *J. Phys. Chem. C* **2010**, *114*, 21555 – 21561.
[26] According to Ref. [13], reaction of O_2^- with water may follow the steps: $O_2^- + H_2O \rightarrow {}^{\bullet}HO_2^{\bullet} + OH^-$; ${}^{\bullet}HO_2 + e^- + H_2O \rightarrow H_2O_2 + OH^-$; $H_2O_2 + e^- \rightarrow {}^{\bullet}OH + OH^-$; ${}^{\bullet}OH + e^- \rightarrow OH^-$.

